



Neuronal Nitric Oxide Synthase Regulates Cerebellar Parallel Fiber Slow EPSC in Purkinje Neurons by Modulating STIM1-Gated TRPC3-Containing Channels

Le Gui¹ · Vasiliki Tellios² · Yun-Yan Xiang¹ · Qingping Feng³ · Wataru Inoue^{1,2,3} · Wei-Yang Lu^{1,2,3}

Accepted: 7 March 2024 / Published online: 12 March 2024

© The Author(s), under exclusive licence to Springer Science+Business Media, LLC, part of Springer Nature 2024

Abstract

Responding to burst stimulation of parallel fibers (PFs), cerebellar Purkinje neurons (PNs) generate a convolved synaptic response displaying a fast excitatory postsynaptic current (EPSC_{Fast}) followed by a slow EPSC (EPSC_{Slow}). The latter is accompanied with a rise of intracellular Ca²⁺ and critical for motor coordination. The genesis of EPSC_{Slow} in PNs results from activation of metabotropic type 1 glutamate receptor (mGluR1), oligomerization of stromal interaction molecule 1 (STIM1) on the membrane of endoplasmic reticulum (ER) and opening of transient receptor potential canonical 3 (TRPC3) channels on the plasma membrane. Neuronal nitric oxide synthase (nNOS) is abundantly expressed in PFs and granule neurons (GNs), catalyzing the production of nitric oxide (NO) hence regulating PF-PN synaptic function. We recently found that nNOS/NO regulates the morphological development of PNs through mGluR1-regulated Ca²⁺-dependent mechanism. This study investigated the role of nNOS/NO in regulating EPSC_{Slow}. Electrophysiological analyses showed that EPSC_{Slow} in cerebellar slices of nNOS knockout (nNOS^{-/-}) mice was significantly larger than that in wildtype (WT) mice. Activation of mGluR1 in cultured PNs from nNOS^{-/-} mice evoked larger TRPC3-channel mediated currents and intracellular Ca²⁺ rise than that in PNs from WT mice. In addition, nNOS inhibitor and NO-donor increased and decreased, respectively, the TRPC3-current and Ca²⁺ rise in PNs. Moreover, the NO-donor effectively decreased TRPC3 currents in HEK293 cells expressing WT STIM1, but not cells expressing a STIM1 with cysteine mutants. These novel findings indicate that nNOS/NO inhibits TRPC3-containing channel mediated cation influx during EPSC_{Slow}, at least in part, by S-nitrosylation of STIM1.

Keywords Cerebellum · Neuronal nitric oxide synthase · Parallel fiber · Slow EPSC · TRPC3 · STIM1

Introduction

The cerebellum is a key brain structure that regulates motor coordination and cognition [1]. In the cerebellar cortex, glutamatergic parallel fibers (PFs) arising from granule neurons (GNs) synapse with the dendritic spines of GABAergic Purkinje neurons (PNs). Integrating excitatory inputs from mossy fibers, GNs discharge action potential bursts, evoking excitatory activities at PF-PN synapses to coordinate motor functions [2, 3]. Responding to burst stimulus of PFs, PNs in cerebellar slices generate convolved EPSCs, displaying a fast component and a slow component respectively, known as fast and slow EPSC (EPSC_{Fast} and EPSC_{Slow}) [4]. Previous studies have demonstrated that EPSC_{Fast} is mediated by AMPA receptors/channels whereas EPSC_{Slow} is initiated by activation of metabotropic type 1 glutamate receptor (mGluR1) [5] and primarily mediated by transient receptor potential

Le Gui and Vasiliki Tellios These authors made equal contributions to this study.

✉ Wataru Inoue
winoue@uwo.ca

✉ Wei-Yang Lu
wlu53@uwo.ca

¹ Robarts Research Institute, University of Western Ontario, 1151 Richmond Street North, London, ON N6A 5B7, Canada

² Graduate Program of Neuroscience, University of Western Ontario, 1151 Richmond Street North, London, ON N6A 5B7, Canada

³ Department of Physiology and Pharmacology, University of Western, Ontario 1151 Richmond Street North, London, ON N6A 5B7, Canada

canonical 3 (TRPC3) [6], a tetrameric non-selective cation channel that conducts Ca^{2+} and Na^{+} influx crossing the plasma membrane [7]. Indeed, deletion of the *Trpc3* gene in mice eliminates the cerebellar EPSC_{Slow} [6] whereas gain-of-function mutation of *Trpc3* in mice increases Ca^{2+} entry to PNs [8], indicating that EPSC_{Slow} in PNs is mediated by TRPC3-containing channels.

Cerebellar PNs express high-level stromal interaction molecule 1 (STIM1) in the endoplasmic reticulum (ER) [9], as well as TRPC3 and TRPC1 [6]. Oligomers of STIM1 in the ER membrane may gate homomeric TRPC3 channels by electrostatic interaction [10] or activate heteromeric TRPC1/3 channels through physical interactions [11]. Accumulated data from previous studies established that activation of mGluR1 in PNs provokes Ca^{2+} release from ER, consequently, mobilizes the Ca^{2+} sensor STIM1 to form oligomers, and activates TRPC3-containing channels to mediate durable $\text{Ca}^{2+}/\text{Na}^{+}$ entry, displaying as EPSC_{Slow}. In other words, STIM1 dimerization or oligomerization is critical for activation of TRPC channels and therefore the genesis of EPSC_{Slow} in PNs, as evidenced by the disappearance of EPSC_{Slow} in STIM1-knockout mice [12]. Early studies showed that the amplitude of EPSC_{Slow} and/or the quantity of Ca^{2+} entry of PNs determine directions of PF-PN synaptic plasticity [13] hence motor coordination [6]. Therefore, aberrant regulations of mGluR1-STIM1-gated TRPC3-containing channel mediated EPSC_{Slow} and Ca^{2+} entry of PNs were associated with various forms of spinocerebellar ataxias [14–16]. However, how the mGluR1-initiated TRPC3-containing channel mediated EPSC_{Slow} is finely regulated remains elusive.

Neuronal nitric oxide synthase (nNOS) is abundantly expressed in PFs/GNs [17], where it catalyzes the production of NO, a diffusible gas molecule that regulates cellular functions primarily by activation of soluble guanylyl cyclase (sGC) or by S-nitrosylation of proteins [18]. It has been well demonstrated that nNOS activity critically modulates the plasticity of PF-PN synapses [19]. For example, mice lacking nNOS expression (nNOS^{-/-}) exhibit abnormalities in PF-PN synaptic plasticity [20] and deficits of motor coordination [21, 22]. Consistently, mutant mice with cerebellar ataxia often exhibit decreased nNOS expression/activity [17]. In line with these early studies, we recently found that PNs in nNOS^{-/-} mice display obvious morphological impairments showing less dendritic spines and fewer synapses, accompanied with significant increase of STIM1 clusters (oligomers) in the soma and dendrites of PNs [23]. Moreover, such morphological alterations of PNs in nNOS^{-/-} mice are related to mGluR1-dependent increase of Ca^{2+} in these cells [23]. All these findings led us to explore whether and how nNOS/NO signaling regulates EPSC_{Slow} in PNs of mice.

Experimental procedures

Voltage-clamp recording in mouse cerebellar slices

Wild type (WT, *C57BL/6*) and nNOS knockout (nNOS^{-/-}, *Nos1^{tm1Pth}/J*) mice were purchased from Jackson Laboratory (Bar Harbor, ME, USA) and a breeding program was implemented at the institutional animal care facility with standard cares. All animal experimental procedures conform to the Canadian Council on Animal Care guidelines for the care and handling of animals and were approved by the Animal Care Committee at Western University under the AUP# 2010–033 and AUP# 2014–031. At postnatal day (P) 18–21, WT and nNOS^{-/-} mice were used to cut parasagittal cerebellar slices as described previously [24] with minor modifications. Briefly, mice were anaesthetized deeply with inhalation of isoflurane (3%) and euthanized by decapitation. The whole brain was quickly dissected out and immersed for 3 min in an ice-cold solution containing the following (in mM): 75 sucrose, 87 NaCl, 25 NaHCO₃, 2.5 KCl, 1.25 NaH₂PO₄, 25 glucose, 7 MgCl₂, 0.5 CaCl₂ (pH 7.4 when bubbled with 95% O₂ and 5% CO₂). Sagittal cerebellar slices (300 μm in thickness) were cut using a vibratome (Leica VT1200s, Leica Biosystems, Concord ON Canada). Slices were then transferred to the artificial cerebrospinal fluid (ACSF) containing the following (in mM): 125 NaCl, 2.5 KCl, 1.25 Na₂HPO₄, 1 MgCl₂, 2 CaCl₂, 26 NaHCO₃, and 25 d-glucose, bubbled with 95% O₂-5% CO₂ maintained at 32 °C and kept there for 45 min. Thereafter, the slices were kept in the same ACSF at room temperature for the rest of the day. To record excitatory synaptic responses, the GABA_AR antagonist picrotoxin (100 μM) was included in ACSF during patch-clamp recordings. A low dose (5 μM) of DNQX was also added to the ACSF in order to partially block AMPA/kainate receptors [25], thus preventing unclamped firing of the cell following a train of synaptic stimulation for evoking slow EPSCs while preserving fast EPSCs in response to paired-pulse stimulation during voltage-clamp recordings [12, 25].

The recording chamber was continuously superfused with ACSF (constantly bubbled with 95% O₂-5% CO₂) at a rate of 1–2 ml/min and maintained at 32 ± 1 °C. PNs in the lobes IV and/or VI were visualized using a 25× or a 40× water-immersion objective attached to an upright microscope (BX51; Olympus, Japan). Under microscopic guidance, motorized micromanipulators (MP225, Sutter) were used to make whole cell patch clamp recordings in somas of PNs located in Lobe IV and VI, where significant changes in morphology, mGluR1 expression, and STIM1 clusters of PNs were identified in nNOS^{-/-} mice by our previous studies [23]. The patch electrodes were pulled

from glass tubes (WPI, Sarasota, FL) by a puller (Narishige, model PP-830). The input resistance of these electrodes was 3–4 M Ω when filled with intracellular solution (ICS) containing (in mM): 116 K-gluconate, 12 Na-gluconate, 8 KCl, 2 MgCl₂, 4 K₂ATP, 0.3 NaGTP, 10 HEPES, 1 EGTA (pH 7.3, adjusted with KOH). After whole-cell configuration, PNs was voltage-clamped at –70 mV. Membrane capacitance of recorded PNs was monitored, and the series resistance was compensated and kept below 25 M Ω under voltage clamp and was auto-bridge balanced in current clamp. To activate PFs, stimulation glass pipettes (~1 μ m tip diameter) were filled with the ACSF and placed in the molecular layer (300–400 μ m away from the recorded PNs). A paired pulse stimulation (50 ms interval) was conducted 2000 ms prior to each trial of the repetitive stimuli to confirm the selective and stable stimulation of PFs [26], while repetitive square pulses (5 to 20 μ A, 200 Hz, 10 pulses) were used to elicit convoluted EPSCs in PNs. Electrical signals recorded from PNs were amplified by means of a Multiclamp 700B amplifier, acquired and filtered at 1 kHz through Digidata 1322A acquisition system, and analyzed using pCLAMP10.3 software (Molecular Devices, Sunnyvale, CA). The averaged trace of 5 EPSCs was stably recorded 8–10 min after whole-cell configuration was used for analyses. To compare the scale of PF-PN slow EPSC between WT mice and nNOS^{-/-} mice, the ratios of slow and fast component of EPSC evoked by repetitive stimuli were calculated as previously reported [12].

To determine the receptors and channels involved in the generation of the PF-PN slow EPSC, the mGluR1 agonist (*S*)-3,5-dihydroxyphenylglycine (DHPG), the mGluR1 selective antagonist JNJ-16259685 (3,4-dihydro-2*H*-pyrano[2,3-*b*]quinolin-7-yl)-(cis-4-methoxycyclohexyl)-methanone) [27]; and Pyrazole 3 (Pyr3), an inhibitor of STIM1-gated TRPC3-containing channels [28], were added to the perfusion ACSF during some recordings. DHPG, JNJ-16259685, and Pyr3 were purchased from Tocris (Balwin, MO).

Immunohistochemistry of mouse cerebellar tissues

Mice aged at P21 were euthanized by decapitation under deep anesthesia using isoflurane. The mouse head was placed in 4% paraformaldehyde (PFA, in PBS) for 24 h and then the brains were removed out of the skull and placed in fresh 4% PFA. After 2-day fixation at 4 °C, the brain was replaced in 30% sucrose (in PBS) for 2–3 days. Cerebella were hemisected through the sagittal line and parasagittal slices were cut at 40–60 μ m thickness using a vibratome. After washing using PBS cerebellar sections were permeabilized with 0.25% Triton X-100 (Sigma) in PBS for 5 min and blocked with 10% normal goat serum (NGS in 0.25% Triton X 100-PBS) for 2 h. After washing, cerebellar sections

were incubated with rabbit anti-TRPC3 (NovusBio, NB110-74935, 1:500) at 4 °C overnight. Sections were washed and then incubated in Cy3-Donkey-anti-rabbit IgG (Jackson ImmunoResearch laboratories Inc., 1:500). For double-staining of PN marker calbindin-D28K, the anti-calbindin-D28K (Santa Cruz Biotechnology, 1:500) and Alexa Fluor® 488-Donkey-anti-goat (Life technologies: 1:1000) were processed. Omission of primary antibody was used as a negative control. The immunostained slices were mounted on glass slides for confocal microscopy using an inverted microscope (Olympus FV1000). To avoid variations in cellular morphology and protein expression in diverse types of cells, confocal microscopy also focused on Lobe IV and VI. Multiple images of immune-stained PNs of cerebellar sections prepared from WT and nNOS^{-/-} mice were taken under 60X oil objective using Olympus Fluoview software and saved in an institute-based data system. The saved images were analyzed using ImageJ (<https://imagej.nih.gov/ij/>). To assess the intensity of TRPC3-fluorescence specifically within PNs, the area of TRPC3-fluorescence overlaid with the fluorescence of calbindin-D28K, the PN marker, was determined; and then the intensity of TRPC3-fluorescence in PNs was measured, as we previously analyzed the fluorescence intensity of proteins in other types of cells [29–32].

Immunoblot of cerebellar tissues

Cerebella from WT and nNOS^{-/-} mice aged P14 or P21 (w2 or w3) were dissected and homogenized using radioimmunoprecipitation (RIPA) buffer with a protein inhibitor cocktail (10 μ g/ml leupeptin and aprotinin; 2 mM phenylmethylsulfonyl fluoride). Protein measurements were determined using a Bradford micro-assay (Bio-Rad) and 40–50 μ g of protein was loaded per well. Proteins were run through SDS-PAGE on either 8% or 10% polyacrylamide gels at 100 V, and then transferred to a nitrocellulose membrane. Membranes were blocked in 5% bovine serum albumin (BSA) in a 1 \times TBS-T solution, and later incubated with primary anti-TRPC3 rabbit antibody (Alomone, ACC-016). Proteins of interest were detected using an anti-guinea pig or anti-rabbit IgG HRP conjugate (Bio-Rad). The immunoblot intensity of TRPC3 protein was normalized to that of β -actin (Sigma, A5441; Abcam, ab9482).

Cultures of primary cerebellar cells

Mixed cerebellar cells were isolated from P3 WT and nNOS^{-/-} mice as previously described [33, 34] with modifications. Briefly, mouse pups were euthanized by decapitation under isoflurane anesthesia. Dissected cerebella were digested with 1% trypsin in Ca²⁺/Mg²⁺ free phosphate-buffered saline (CMF-PBS) for 3 min at room temperature and triturated to yield single cell suspension. The suspension

passed through a 33 μm nylon mesh and single cells were re-suspended in serum-containing medium was composed of Eagle's basal medium with Earle's salts, glutamine, glucose, penicillin–streptomycin, and 10% horse serum (Life Technologies) in 35 mm culture dishes, which were pre-treated overnight at 4 °C with poly-D-lysine (PDL, 500 $\mu\text{g}/\text{ml}$; Sigma) and washed three times with distilled water before plating. These mixed cerebellar cells obtained from WT and nNOS^{-/-} mice respectively were cultured in serum-free medium and maintained at 37 °C with 100% humidity and 5% CO₂. Three hours after plating, the morphologies of primary cerebellar cells in cultures were checked under microscope. By twenty-four hours, PNs in the cultures could be readily identified under microscope because of their large soma and multiple dendrites. Specifically, individual PNs scattered among granule cells. Consistent with previous reports [33, 34], PNs represented 1%–3% of cell population in the cultures where the majority were nNOS-expressing GNs [17] that display small round soma.

Voltage-clamp recording in cultured mouse PNs

Forty-eight hours after culturing, cells were rinsed with and bathed in the extracellular solution (ECS) containing (in mM): 126 NaCl, 4 KCl, 2.0 CaCl₂, 1.0 MgCl₂, 10 HEPES, and 15 glucose, 0.0005 tetrodotoxin, 0.01 nifedipine, and 0.001 ω -conotoxin GVIA (pH = 7.4 and osmolarity = 320 mosmol/L), then were used for patch-clamp recordings in room temperature. In some recordings, NNC 55–0396 dihydrochloride (300 μM), a selective T-type calcium channel blocker [35] was included in ECS. PNs in the cultures of cerebellar cells from WT and nNOS^{-/-} mice were identified under microscope based on their unique morphology. Whole-cell configuration was performed on the somas of PNs using glass pipette electrodes. Input resistance of glass electrodes was within the range of 2–4 M Ω when the pipette was filled with intracellular solution (ICS) containing (in mM): 120 Cs-gluconate, 1 MgCl₂, 4 Na₂ATP, 1 NaGTP, 20 Hepes, 10 EGTA and 5 sucrose (pH 7.3, adjusted with CsOH). Under whole-cell voltage-clamp mode ($V_{\text{H}} = -70$ mV), series resistance was maintained below 10–12 M Ω . The current–voltage relationship of transmembrane conductance was revealed by a voltage-ramp (V_{Ramp} , from -100 mV to 20 mV within 3 s) when PNs were clamped at 0 mV. Specifically, the level of transmembrane conductance in test PNs was examined when they were perfused with the control solution, solution containing the mGluR1 agonist DHPG (250 μM), and solution containing DHPG (250 μM) + TRPC3-containing channel inhibitor Pyr3 (2.0 μM), respectively. Readings of control and the mGluR1-evoked TRPC3 conductance in individual test PNs were derived by deducting the transmembrane conductance recorded in the presence of Pyr3 from the transmembrane

conductance recorded in control conditions and/or in the presence of DHPG.

Imaging cytosolic Ca²⁺ in cultured mouse PNs

Forty-eight hours after growing in cultures, primary cerebellar cells on 35 mm glass bottom dishes were washed using the same bath solution for patch-clamp recording, and incubated with 3 μM Rhod-4 AM (AAT Bioquest, Sunnyvale, CA) for 30 min in 30°C, and then excess Rhod-4 AM was washed out. Under Olympus FV1000 microscope at $\times 20$ magnification, images of Ca²⁺-dependent Rhod-4 fluorescence in primary cerebellar cells were automatically taken every 3 s using a computerized program, and automatically recorded in a computer. In different cell cultures, baseline levels of Ca²⁺-dependent fluorescence were recorded 3–5 min before perfusion of DHPG, Pyr3, the selective nNOS inhibitor 7-nitroindazole (7N), and the fast release NO-donor S-nitroso-N-acetyl penicillamine (SNAP), respectively. Some PNs, in particular those closely surrounded by clusters of GNs, displayed irregular Rhod-4 fluorescence fluctuations, which might reflect PNs' response to burst release of glutamate from GNs. The images of Rhod-4 fluorescence were analyzed off-line. PNs in the image field were visibly identified by their large soma and higher basal Rhod-4 fluorescence compared to surrounding GNs. Using the FIJI open-source software [36], the intensity of Ca²⁺-dependent Rhod-4 fluorescence within PNs before and after application of GHPG were automatically measured and digitized. The readings of drug-induced Rhod-4 fluorescence change within all PNs were normalized to the baseline level (before DHPG). Using Excel, the values of mean \pm SE of normalized intensity of Ca²⁺-dependent Rhod-4 fluorescence in all PNs in the image field were plotted along with the imaging time.

Voltage-clamp recording in transfected cells

HEK293 cells were grown in Dulbecco's Modification of Eagle's Medium plus 10% fetal bovine serum. In 60% confluence, the cells were co-transfected with pCMV6 vector encoding human TRPC3 tagged with GFP (NM_003305, OriGene Technologies, Rockville, MD USA) and pCMV6 vector encoding human STIM1 or encoding Cys49Ser/Cys56Ser mutations, with mCh fused just after the ER signal peptide [37]. The Cys49Ser/Cys56Ser mutations were introduced using the QuikChange method. Cells were transfected using an Amaxa Nucleofector II following the manufacturer's guidelines using 0.5 μg eGFP-TRPC3 and mCh-STIM1 or Cys49Ser/Cys56Ser mCh-STIM1. Twenty-four hours after transfection, cells were replated on 35 mm dish coated with poly-D-lysine. Twelve to twenty-four hours after replating, transfected cells were bathed in ECS containing (in

mM): 126 NaCl, 4 KCl, 2.0 CaCl₂, 1.0 MgCl₂, 10 HEPES, and 12 glucose (pH = 7.4, and osmolarity = 320 mosmol/L). Whole-cell recording was performed on the transfected cells that were identified under microscope-associated fluorescence filters in room temperature using another recording set that were also equipped with Multiclamp 700B amplifier and pCLAMP10.3 for acquisition (Molecular Devices). The input resistances of glass pipette electrodes were 2–3 MΩ when filled with ICS containing (in mM): 120 Cs-gluconate, 1 MgCl₂, 4 Na₂ATP, 1 NaGTP, 20 Hepes, 10 EGTA and 5 sucrose. Under voltage-clamp mode ($V_H = 70$ mV), whole-cell series resistance was 8–10 MΩ. Once series resistance became stable the recorded cell was clamped at 0 mV, and the transmembrane current and current–voltage relationship were revealed by applying V_{Ramp} from -100 mV to 20 mV within 3 s. The series resistance was monitored, and the recording excluded once it surpassed 12 MΩ.

Statistical analysis

Statistical analyses were performed using an unpaired, two-tailed t test for comparing all results from PNs between WT to nNOS^{-/-} mice. When comparing results of immunocytochemistry, immunoblot, and Ca²⁺-imaging from three or more groups were analyzed using a one-way analysis of variance (ANOVA) corrected with a Tukey's post hoc test. Significance was determined using a threshold of $p = 0.05$. All values are reported as mean ± SEM.

Results

Enlarged slow EPSC in PNs of nNOS^{-/-} mice

In cerebellar slices prepared from WT mice, paired pulse stimulation of PFs in the molecular layer elicited paired-pulse response (PPR) in PNs, which displayed as a smaller EPSC1 and a larger EPSC2. As shown in the left panel of Fig. 1A, this profile of PPR exhibited an archetype of paired-pulse-facilitation (PPF), confirming that it was a response of PF-PN synapses [26]. In addition, a burst stimulation (200 Hz, 10 pulses) of the same loci induced a convoluted EPSC. As shown in the right panels of Fig. 1A, this complex EPSC in PNs was characterized with a fast component (EPSC_{Fast}) followed by a long-lasting slow component (EPSC_{Slow}). Consistent with previous report [38], the amplitude of EPSC_{Slow} was effectively decreased in 2 PNs of WT cerebella and 3 PNs of nNOS^{-/-} cerebella by bath application of the mGluR1 antagonist JNJ16259685 (30 μM). However, this mGluR1 antagonist did not change the amplitude of EPSC_{Fast}. This result confirmed that EPSC_{Slow}, but not EPSC_{Fast}, is initiated by mGluR1 activation [5]. As shown in Fig. 1B, paired pulse stimulation

of PFs in the molecular layer of cerebellar slices from nNOS^{-/-} mice also elicited PPF, while burst stimulation (200 Hz, 10 pulses) induced a convoluted EPSC. The amplitude of EPSC1 and EPSC2, as well as EPSC_{Fast} and EPSC_{Slow} in PNs of both WT and nNOS^{-/-} mice remained stable over 10–15 min recording. Notably, in response to paired pulses and/or burst stimulations, PNs in both WT and nNOS^{-/-} cerebella displayed similar levels of PPF (Fig. 1C, WT: EPSC2/EPSC1 = 1.63 ± 0.83, n = 7; nNOS^{-/-}: EPSC2/EPSC1 = 1.32 ± 0.23, n = 9), suggesting that deficiency of NO signaling did not fundamentally alter vesicular glutamate release from the presynaptic PF terminals.

Burst stimulations of PFs in the same loci of molecular layer readily induced convoluted EPSCs, which displayed comparable amplitudes of EPSC_{Fast} in WT and nNOS^{-/-} cerebella (WT: 332 ± 59 pA, n = 9 cells vs. nNOS^{-/-}: 295 ± 25 pA, n = 11 cells). However, as illustrated in the right panel of Fig. 1B the amplitude of EPSC_{Slow} in nNOS^{-/-} cerebella was drastically larger than that in WT cerebella (Fig. 1D; WT: 59 ± 21 pA, n = 9 cells vs. nNOS^{-/-}: 158 ± 21 pA, n = 11 cells; $P < 0.005$). Remarkably, the ratio of EPSC_{Slow}/EPSC_{Fast} in PNs of nNOS^{-/-} mice was more than two times bigger than that in WT mice (Fig. 1E, WT: 0.173 ± 0.036, n = 9 cells from 5 mice; nNOS^{-/-}: 0.476 ± 0.094, n = 11 cells from 5 mice, $P < 0.01$). As illustrated in the right panel of Fig. 1B, application of Pyr3 (3.0 μM), an inhibitor of STIM1-gated TRPC3-containing channels [39], greatly reduced the amplitude of EPSC_{Slow} (Fig. 1F; control: 141 ± 34 pA vs. Pyr3: 34 ± 15 pA, n = 5 cells, $p < 0.01$), but not the EPSC_{Fast} in PNs of nNOS^{-/-} mice. The same effect of Pyr3 (3.0 μM) was also observed in two PNs of WT mice. In consistence with previous findings [6], this result implicates that STIM1-gated TRPC3-containing channels are critically involved in the genesis of EPSC_{Slow} of PNs.

Together, these results indicate that endogenous nNOS/NO signaling in the cerebellum controls PF-PN synaptic responses by effectively downregulating mGluR1-initiated TRPC3-channel activity in PNs.

Mild decrease in TRPC3 protein in PNs of nNOS^{-/-} mice

Does NO signaling downregulate TRPC3 channel activity by decreasing the expression of TRPC3 protein in PNs? Immunohistochemistry and confocal microscopy of cerebellar sections revealed immunofluorescence of TRPC3 protein in the soma and dendrites of PNs of both WT and nNOS^{-/-} mice at postnatal week-3 (Fig. 2A). Image analyses revealed a mild but significant decrease of TRPC3-fluorescence intensity in PNs of nNOS^{-/-} cerebella relative to that WT cerebella (Fig. 2B). Considering that the TRPC3 expression profile in the cerebellum is not homogeneous [40], we also

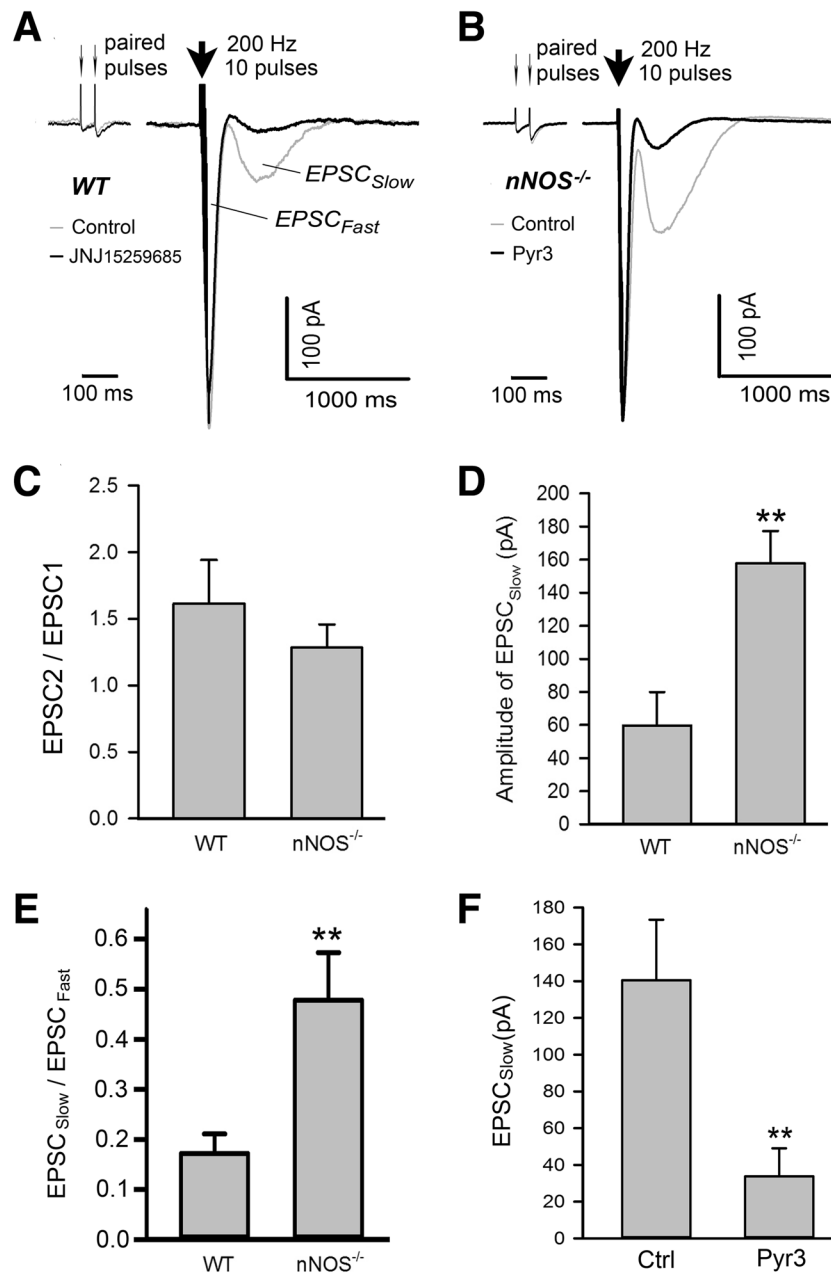


Fig. 1 Increased slow EPSCs in PNs of *nNOS*^{-/-} mice. **A.** Example traces of evoked EPSCs of PF-PN synapse in responses to a paired pulse stimulation followed by a brief burst stimulation (10 pulses, 200 Hz) in a cerebellar slice of WT mice before (grey trace) and after perfusion of the mGluR1 antagonist JNJ16259685 (black trace). Paired pulses induced paired-pulse-facilitation (PPF, left panel) confirming the selective stimulation of PFs; whereas burst stimulation evoked large complex EPSCs displaying a fast component and a slow component of EPSC (EPSC_{Fast} and EPSC_{Slow}) sequentially (right panel). Note that the mGluR1 inhibitor JNJ16259685 (30 μ M) effectively decreased the EPSC_{Slow} but not the EPSC_{Fast} nor the PPF. **B.** Shown are example traces of PPF (left panel) as well as EPSC_{Fast}

and EPSC_{Slow} (right panel) recorded from a PN in a *nNOS*^{-/-} cerebellar slice before (grey trace) and after (black trace) application of Pyr3 (3.0 μ M), an antagonist for STIM1-gated TRPC channels. Note that Pyr3 blocked EPSC_{Slow} but not EPSC_{Fast}. **C.** Plotted graph shows no significant difference in the ratio of paired-pulse induced EPSC2/EPSC1 between WT mice and *nNOS*^{-/-} mice. **D.** Plots report larger amplitudes of EPSC_{Slow} in PNs of *nNOS*^{-/-} mice than WT mice between WT mice and *nNOS*^{-/-} mice (** $P < 0.01$). **E.** Bars summarize the average ratio of EPSC_{Slow} vs. EPSC_{Fast} in WT and *nNOS*^{-/-} mice (** $P < 0.005$). **F.** Plots show the average amplitude of EPSC_{Slow} in PNs of *nNOS*^{-/-} mice before and after application of Pyr3 (** $P < 0.01$)

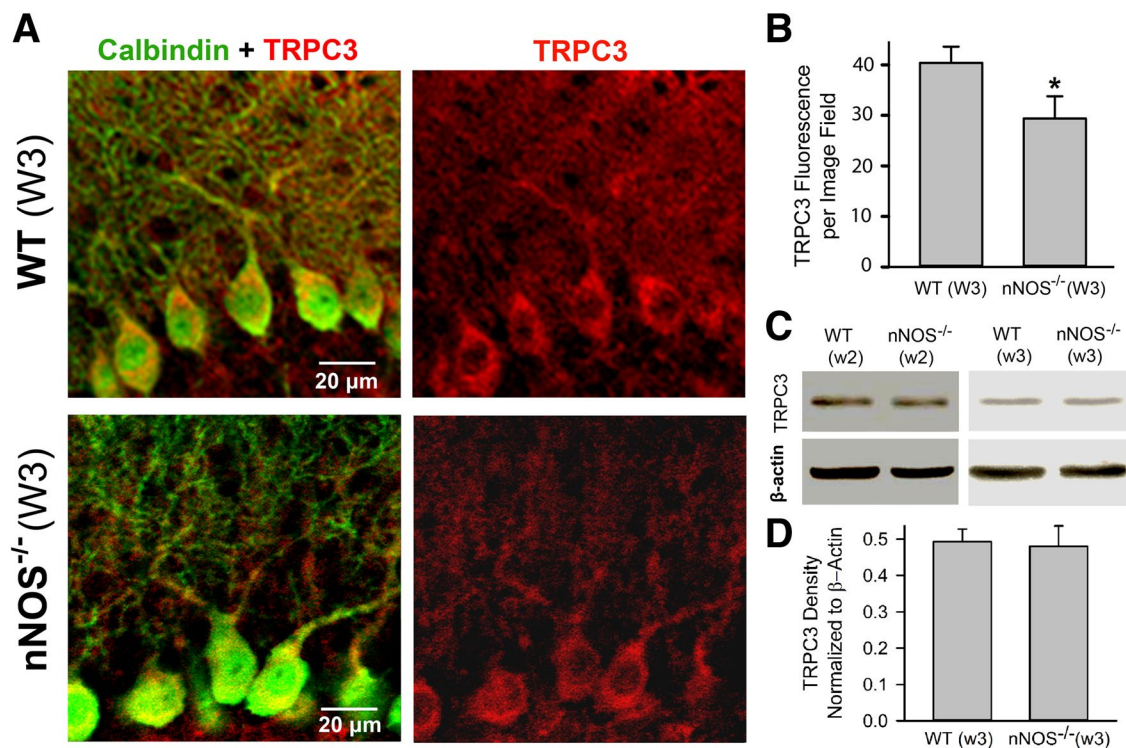


Fig. 2 Mild decrease in TRPC3 expression in PNs of *nNOS*^{-/-} mice. **A.** Representative images display immunofluorescence of calbindin-D28K (green) as well as TRPC3 (red) within PNs located in the Lobe IV of WT mouse (upper row) and *nNOS*^{-/-} mouse (lower row) at postnatal week-3. Note the strong immunofluorescence of TRPC3 in the calbindin-D28K⁺ dendrites and somas of PNs in both WT and *nNOS*^{-/-} cerebella. To selectively assess the intensity of TRPC-fluorescence within PNs, the area of TRPC3-fluorescence overlaid with the calbindin-D28K fluorescence was determined; and then the intensity of TRPC3-fluorescence only within PNs was measured. **B.** Plotted graph summarizes arbitrary units of TRPC3 fluorescence

associated with the dendrites and somas of PNs per image field (15 images of cerebellar slices from 5 WT mice and 12 images of cerebellar slices from 4 *nNOS*^{-/-} mice; $P < 0.05$). **C.** Example immunoblots for TRPC3 (~95 kDa) and β -actin (loading control) of the whole cerebellar tissues from WT mouse and *nNOS*^{-/-} mouse at postnatal week-2 (left column) and at postnatal week-3 (right column). **D.** Plots summarize quantification of protein blots showing no significant difference in normalized TRPC3 protein density in whole cerebellar tissues between WT mice ($N = 4$ cerebella from 4 mice at week-3) and *nNOS*^{-/-} mice ($N = 4$ cerebella from 4 mice at week-3)

carried out immunoblotting assays of the whole cerebellar cortical tissues from WT and *nNOS*^{-/-} mice at postnatal week-2 and week-3. Results from immunoblotting assays, however, showed no significant difference in TRPC3 protein expression between WT and *nNOS*^{-/-} mice at postnatal week-3 (Figs. 2C and D). These results suggested that amplification of the mGluR1-initiated TRPC3-mediated EPSC_{slow} in *nNOS*^{-/-} mice is not due to increased expression of TRPC3 in PNs.

Enlarged mGluR1-activated TRPC3 conductance in cultured PNs from *nNOS*^{-/-} mice

Next, we conducted voltage-clamp recordings on individual PNs in the cultures of mixed primary cerebellar cells isolated from WT and *nNOS*^{-/-} mice. To reveal the mGluR1-initiated TRPC3-mediated transmembrane conductance/current, a V_{Ramp} (from -100 mV to 20 mV) was applied to test PNs when it was perfused with the control solution,

solution containing DHPG (100 μM), and solution containing DHPG (100 μM) and Pyr3 (2.0 μM), respectively. Notably, under control conditions, low-level membrane conductance/current was revealed by V_{Ramp} in cultured PNs from WT mouse (Fig. 3A) and *nNOS*^{-/-} mouse (Fig. 3B). Plotting the transmembrane current against V_{Ramp} revealed a linear voltage-current (I-V) relationship with the reversing potential at 0 mV, indicating that endogenous non-selective cation conductance exists in PNs.

The amplitude of non-selective cation conductance in cultured PNs from both WT mice (Figs. 3A and C) and *nNOS*^{-/-} mice (Figs. 3B and D) was enhanced by application of DHPG, a selective agonist for mGluR1/5. Given that mGluR1 overrides but mGluR5 is undetectable in PNs [41], the effect of DHPG in cerebellar PNs should be attributed to activation of mGluR1. Notably, in the presence of the same concentration of DHPG, the cation conductance in cultured PNs from *nNOS*^{-/-} mice was significantly larger than that in PNs from WT mice. In contrast, application of

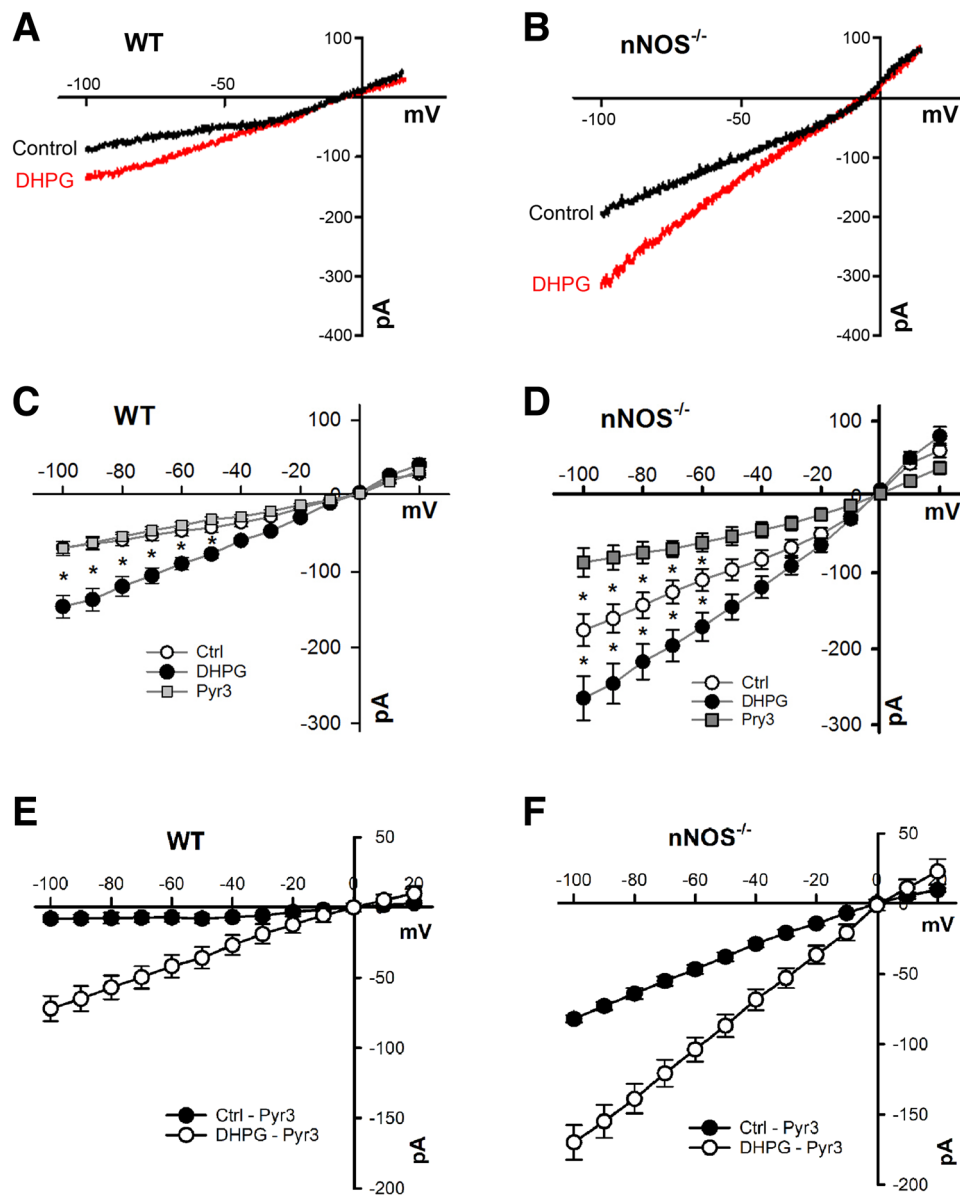


Fig. 3 Increased TRPC3 conductance in PNs of *nNOS*^{-/-} mice. **A–B.** Shown are representative traces of V_{Ramp} -evoked transmembrane-conductance in a cultured PN from a WT mouse (**A**) and in a PN from a *nNOS*^{-/-} mouse (**B**) when the test PN was bathed with control solution and then in the presence of DHPG (100 μM). **C.** Plotted graph shows the current–voltage (I–V) relationship of V_{Ramp} -evoked transmembrane-conductance in PNs ($n=12$ cells) from WT mice in control, or presence of 100 μM DHPG, or 100 μM DHPG+2.0 μM Pyr3 (* at the indicated holding membrane potentials, transmembrane current was significantly different [$P<0.05$] when test PN was exposed to DHPG vs. DHPG+Pyr3). **D.** Plotted graph shows the current–voltage (I–V) relationship of V_{Ramp} -evoked transmembrane-conductance in PNs ($n=8$ cells) from *nNOS*^{-/-} mice in control, or presence of 100 μM DHPG, or 100 μM DHPG+2.0 μM Pyr3 (* at the indicated holding membrane potentials, transmembrane current

was significantly different [$P<0.05$] when test PN was exposed to DHPG vs. DHPG+Pyr3). **E–F.** Shown are “basal TRPC3 current” and “mGluR1-evoked TRPC3 current” in test PNs from WT mice (**E**) and from *nNOS*^{-/-} mice (**F**). Plotted values of “basal TRPC3 current” and “mGluR1-evoked TRPC3 current” were obtained by deducting the conductance when PNs were bathed in Pyr3, from the conductance when PNs were bathed in control (Ctrl) solution and/or in the presence of DHPG, respectively. Note: when $V_{\text{H}}=0$ mV, basal TRPC3 current in PNs from WT mice (**E**) is 7.3 ± 3.3 pA ($n=13$ cells) whereas that in PNs from *nNOS*^{-/-} mice (**F**) is 50 ± 3.3 pA ($n=10$ cells), $P<0.005$. When $V_{\text{H}}=-70$ mV, the mGluR1-evoked TRPC3 current in PNs from WT mice (in **E**) is 55 ± 3.3 pA ($n=13$ cells) whereas that in PNs from *nNOS*^{-/-} mice (in **F**) is 121 ± 9.6 pA ($n=10$ cells), $P<0.001$

Pyr3, an inhibitor of TRPC3-containing channels, decreased the non-selective cation conductance in PNs from both WT mice (Fig. 3C) and $nNOS^{-/-}$ mice (Fig. 3D) to a similar level. These results indicated that the mGluR1-evoked non-selective cation conductance in PNs is mediated by TRPC3-containing channels.

We further dissected the TRPC3 conductance in PNs from WT mice and $nNOS^{-/-}$ mice by deducting the current recorded in the presence of Pyr3, from the current recorded when cells were bathed in control solution and/or DHPG-containing solution, respectively. As shown in Figs. 3E and F, both the basal TRPC3 conductance and the DHPG-evoked TRPC3 conductance in PNs from $nNOS^{-/-}$ mice were larger than that in PNs from WT mice. Notably, both the basal TRPC3 conductance (Fig. 3E) and the DHPG-enhanced conductance (Fig. 3F) in PNs from $nNOS^{-/-}$ mice are larger than that in PNs from WT mice. This result indicates that endogenous NO effectively downregulates the mGluR1-evoked TRPC3 channels. Interestingly, at the same concentration the mGluR1 agonist DHPG evoked a significantly larger conductance in PNs from $nNOS^{-/-}$ mice than that from WT mice (Figs. 3A–D).

This result implies that endogenous NO can downregulate the activity level of mGluR1-sensitive TRPC3 channels through signaling mechanism(s) within individual PNs.

Our previous studies showed that the immunofluorescence clusters of STIM1 oligomers significantly increased in PNs of $nNOS^{-/-}$ mice compared to that of WT mice [23]. We therefore explored whether $nNOS/NO$ signaling regulates the mGluR1-initiated TRPC3 channel activity by modulating STIM1-gated TRPC channels. Results showed that in the presence of DHPG (100 μ M), adding SKF96365 (10 μ M), an inhibitor of STIM1-operated channels [42] to the bath solution greatly decreased the amplitude of TRPC3 conductance in both WT and $nNOS^{-/-}$ PNs (Figs. 4A and B). In the presence of DHPG, adding the NO donor GSNO (250 μ M) to the bath also significantly decreased the amplitude of TRPC3 conductance in WT and $nNOS^{-/-}$ PNs (Figs. 4C and D). These results suggested that the mGluR1-initiated activation of TRPC3 channels in PNs is related to STIM1 mobilization and TRPC3-channel activation, and this process is effectively downregulated by NO signaling.

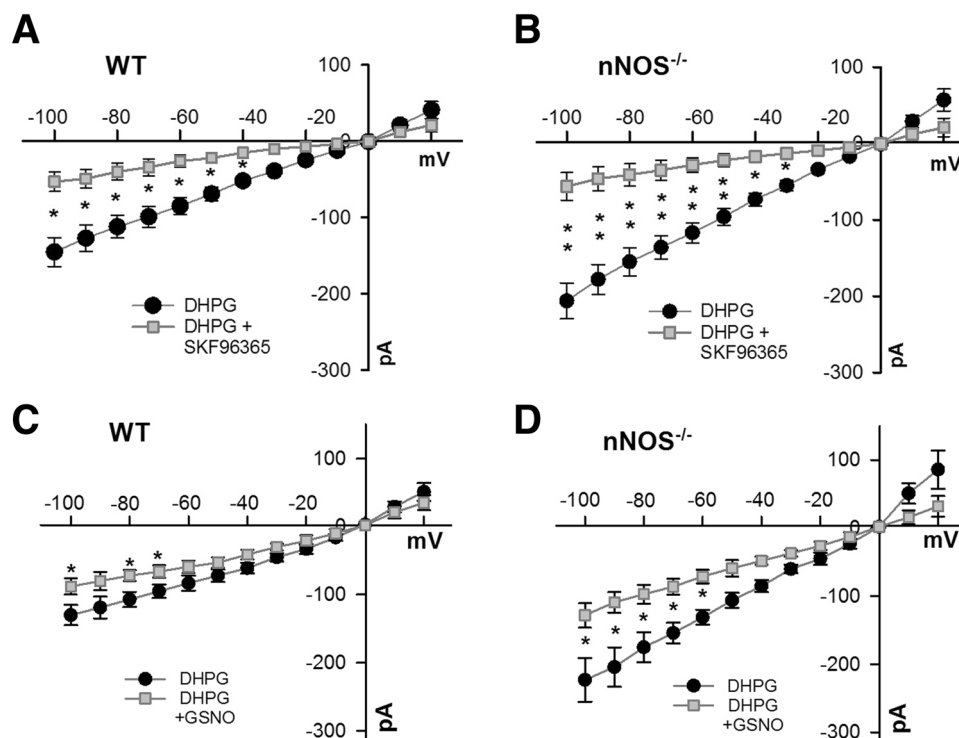


Fig. 4 TRPC3 currents in PNs from WT mice were reduced by mGluR1 inhibitor and NO-donor. **A–B.** Graph summarizes the V_{Ramp} -revealed conductance of PNs isolated from WT mice (**A**) and from $nNOS^{-/-}$ mice (**B**) treated with DHPG (100 μ M) alone or with DHPG plus SKF96365 (10 μ M), a blocker of STIM-gated channels. In WT PNs (**A**) when $V_H = -80$ mV, DHPG: 112 ± 15 pA, $n = 6$ cells, vs. DHPG + SKF96365: 40 ± 115 pA, $n = 5$ cells, $*P < 0.05$. In $nNOS^{-/-}$ PNs (**B**) when $V_H = -80$ mV, DHPG: 155 ± 18 pA, $n = 5$

cells, vs. DHPG + SKF96365: 41 ± 14 pA, $n = 5$ cells, $*P < 0.05$. **C–D.** Graph summarizes the V_{Ramp} -revealed conductance of PNs isolated from WT mice (**C**) and from $nNOS^{-/-}$ mice (**D**) treated with DHPG alone or with DHPG + 250 μ M GSNO, a NO-donor. In WT PNs (**C**) when $V_H = -80$ mV, DHPG: 107 ± 7.3 pA, $n = 8$ cells, vs. DHPG + GSNO: 72 ± 8 pA, $n = 8$ cells, $*P < 0.05$. In $nNOS^{-/-}$ PNs (**D**) when $V_H = -80$ mV, DHPG: 175 ± 22 pA, $n = 8$ cells, vs. DHPG + GSNO: 97 ± 14 pA, $n = 8$ cells; $*P < 0.05$

NO signaling restrains intracellular Ca^{2+} rise in PNs

Our previous studies also showed that NO deficiency causes fundamental impairments of morphology of PNs in $\text{nNOS}^{-/-}$ mice through an mGluR1 -dependent increase of intracellular Ca^{2+} [23]. We therefore examined whether NO signaling restrains intracellular Ca^{2+} levels in PNs. Specifically, we imaged the Ca^{2+} -dependent Rhod-4 fluorescence within PNs that presented in cultures of mixed cerebellar cells from WT and $\text{nNOS}^{-/-}$ mice. As shown in Figs. 5A and B, adding the mGluR1 agonist DHPG (100 μM) to the bath solution evoked a rapid and long-lasting rise of Ca^{2+} in cultured PNs from WT mice. The DHPG-evoked rise of intracellular Ca^{2+} was effectively inhibited by the TRPC3 inhibitor Pyr3 (2.0 μM). Notably, this DHPG-evoked Ca^{2+} rise in PNs was enhanced by inhibiting nNOS using 7-nitroindazole (7N, 50 nM) (Fig. 5A). In contrast, the DHPG-evoked Ca^{2+} rise in PNs was drastically reduced in the presence of S-nitroso-N-acetyl penicillamine (SNAP, 250 μM), a fast-release NO donor (Figs. 5C and D). Together, these

results confirm that nNOS/NO signaling indeed restrains the mGluR1 -initiated TRPC3-mediated Ca^{2+} entry to PNs.

NO donor decreases the TRPC3 conductance in cells expressing WT STIM1, but not in cells expressing mutant STIM1

Increased immune clusters (oligomers) of STIM1 in PNs of $\text{nNOS}^{-/-}$ mice [23] implies that endogenous nNOS/NO signaling in the cerebellum restrains STIM1 oligomerization hence decreasing the interactions between oligomerized STIM1 and STIM1-gated channels such as Orai and TRPC3-containing channels in the plasma membrane. In this regard, we have demonstrated that NO inhibits oligomerization of STIM1 by S-nitrosylation its Cys49 and Cys56 residues thus downregulating the activity of store-operated Orai1-formed Ca^{2+} channels in mouse cardiomyocytes [43]. We therefore examined whether NO downregulates TRPC3-channel activity in PNs also by S-nitrosylation of Cys49 and Cys56 residues on STIM1. To this aim, we made whole-cell

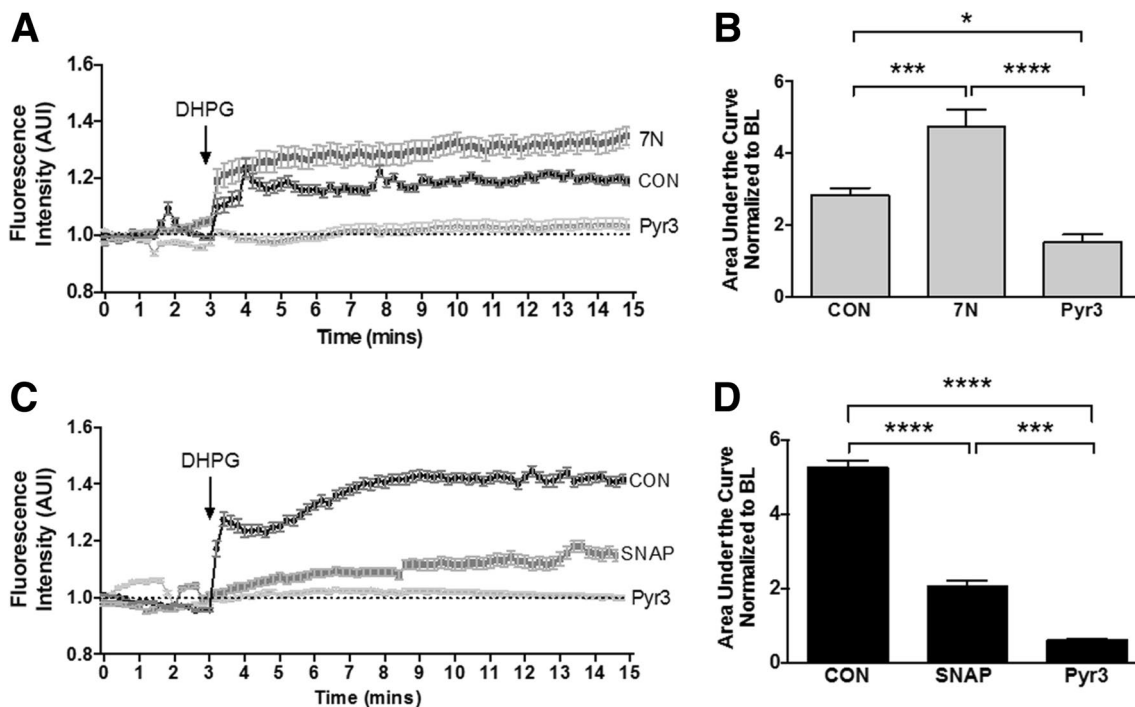


Fig. 5 NO signaling regulates mGluR1 -evoked intracellular Ca^{2+} in cultured PNs. **A.** Plotted traces show DHPG (100 μM)-induced changes of arbitrary unit intensity (AUI) of Rhod4 fluorescence within multiple PNs in three separated cerebellar cultures ($n=9-14$ PNs) that were bathed with the control solution, or solutions containing the nNOS inhibitor 7-nitroindazole (7N, 50 nM), or Pyr3 (2.0 μM), respectively. **B.** Plotted graph shows the arbitrary areas under the Rhod4 fluorescence rising curve of all PNs during 12 min after DHPG application under three different test conditions described in A. Note that the DHPG-evoked rise of Ca^{2+} within PNs was enhanced by the nNOS inhibitor 7N but eliminated by the

STIM1-gated TRPC3-containing inhibitor Pyr3. **C.** Plotted traces show DHPG-induced changes of arbitrary unit intensity (AUI) of Rhod4 fluorescence within multiple PNs in three separated cerebellar cultures ($n=8-12$ PNs) that were bathed with the control solution, or solutions containing the fast-release NO-donor SNAP (250 μM), or solution containing Pyr3 (2.0 μM), respectively. **D.** Plotted graph shows the areas under the Rhod4 fluorescence rising curve of all PNs during 12 min after DHPG application under three different test conditions described in C. Note that the DHPG-evoked Ca^{2+} rise in PNs decreased in the presence of NO donor, and almost disappeared in the presence of Pyr3 (2.0 μM)

voltage-clamp recordings in HEK293 cells expressing TRPC3 and WT STIM1 and in HEK293 cells expressing TRPC3 and STIM1 with Cys49Ser/Cys56Ser mutations. V_{Ramp} (from -100 mV to 20 mV, 3 s) revealed non-selective cation conductance (evidenced by linear I-V relationship)

in cells expressing TRPC3+ WT STIM1 (Fig. 6A) and in cells expressing TRPC3+ STIM1 mutant (Fig. 6B). Bath application of Pyr3 (1.0 μ M), an inhibitor for STIM1-gated TRPC3-containing channels, decreased partially but significantly the non-selective cation conductance in cells

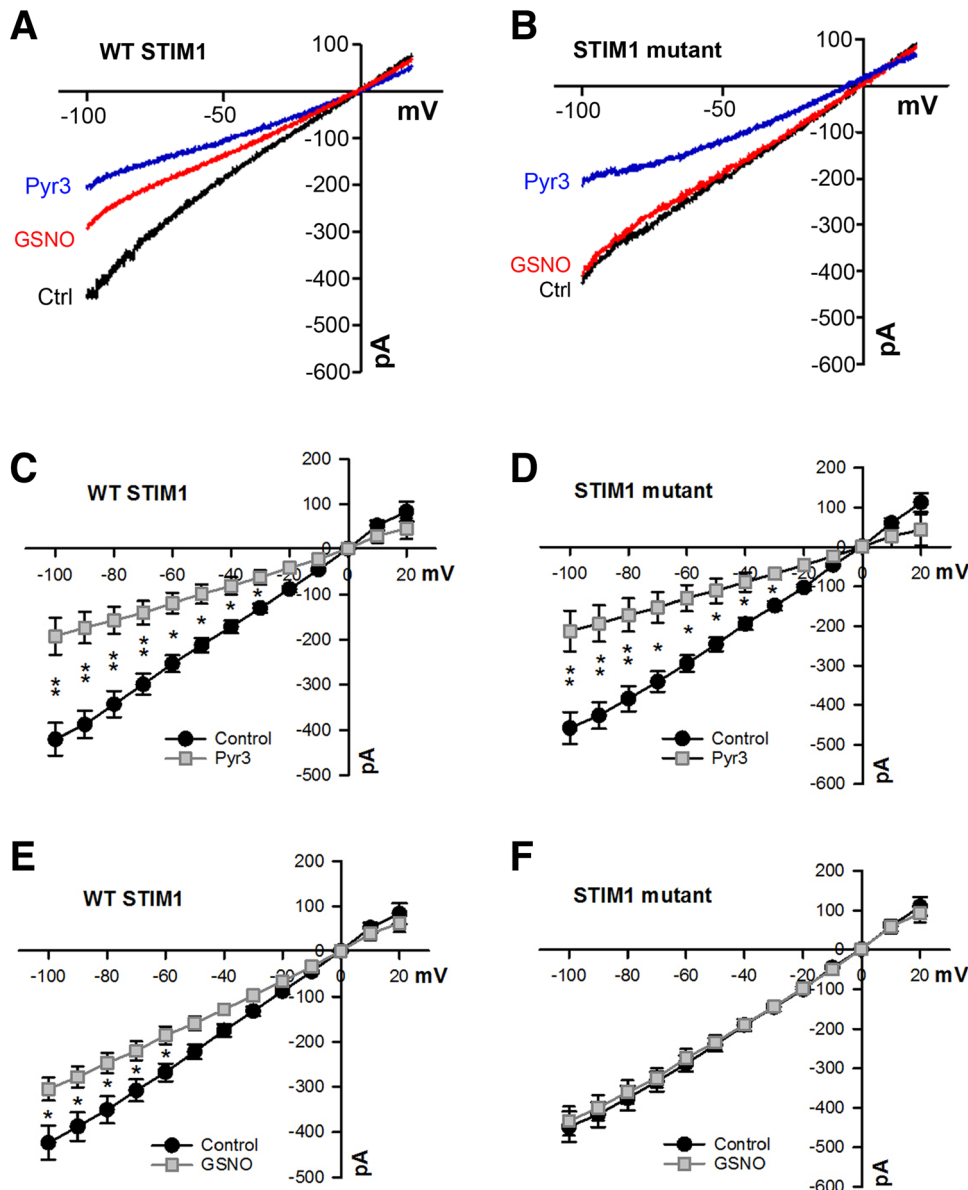


Fig. 6 NO-donor decreases the TRPC3-mediated current in HEK293 cells co-expressing TRPC3 and WT STIM1, but not in cells co-expressing TRPC3 and STIM1 mutant. **A-B.** Example traces of transmembrane conductance elicited in a HEK293 cell co-expressing TRPC3+STIM1 (**A**) and a HEK293 cell co-expressing TRPC3+STIM1 mutant (**B**) by a voltage ramp (-100 mV to 20 mV) before (-GSNO), after adding 250 μ M GSNO (+GSNO), and then adding 1.0 μ M Pyr3 (+Pyr3) to the perfusion bath. **C.** Graph summarizes effect of Pyr3 (1.0 μ M) on the V_{Ramp} -revealed conductance in cells expressing TRPC3+WT STIM1 (at V_H = -80 mV, control: 343 \pm 29pA vs. Pyr3: 157 \pm 30pA, n=6 cells; * P < 0.05 and

** P < 0.01). **D.** Graph summarizes effect of Pyr3 (10 μ M) on the V_{Ramp} -revealed conductance in cells expressing TRPC3+STIM1 mutant (at V_H = -80 mV, control: 384 \pm 32pA, vs Pyr3: 172 \pm 42pA, n=5 cells; * P < 0.05 and ** P < 0.01). **E.** Graph summarizes effect of GSNO (250 μ M) on the V_{Ramp} -revealed conductance in cells expressing TRPC3+WT STIM1 (at V_H = -80 mV, control: 351 \pm 31pA, vs. GSNO: 247 \pm 22pA, n=6 cells; * P < 0.05). **F.** Graph summarizes effect of GSNO (250 μ M) on the V_{Ramp} -evoked conductance in cells expressing TRPC3+STIM1 mutant (at V_H = -80 mV, control: 358 \pm 16pA, vs. +GSNO: 331 \pm 16pA, n=5 cells)

expressing TRPC3 + WT STIM1 (Fig. 6C) and in cells expressing TRPC3 + STIM1 mutant (Fig. 6D). This result implies that in addition to the transfected TRPC3 channels, HEK293 cells express Pyr3-insensitive non-selective cation channels as previously reported [44]. Notably, adding GSNO (250 μ M) to the bath solution partially but significantly decreased the amplitude of non-selective cation conductance in cells expressing TRPC3 + WT STIM1 (Fig. 6E) but had no effect in cells expressing TRPC3 + STIM1 mutant (Fig. 6F). These results suggested that NO inhibits STIM1-gated TRPC3-containing channels by modulating S-nitrosylation of Cys49 and Cys56 residues of STIM1.

Discussion

Previous studies have demonstrated that in the cerebellum, GNs and PFs, as well as basket and stellate interneurons, express high levels of nNOS and produce large volumes of NO, a gaseous molecule that induces signaling in the NO-producing cells and the neighboring cells [45]. In addition, EPSC_{Slow} in PNs is instigated by mGluR1 activation and mediated by STIM1-gated TRPC3-containing channels, which controls essential functions of the cerebellum. The present study reports novel findings that endogenous NO signaling in mouse cerebellum critically restrains the amplitude of EPSC_{Slow} and the activity level of mGluR1-evoked TRPC3-containing channels in PNs, at least partially, by S-nitrosylation of Cys49 and Cys56 residues of STIM1.

Consistent with early studies, our results confirmed that EPSC_{Slow} in PNs is initiated by mGluR1 activation and mediated by STIM1-gated TRPC3-containing channels, evidenced by the findings that EPSC_{Slow} in cerebellar PNs (Figs. 1A) and the mGluR1-evoked non-selective cation conductance in cultured PNs (Figs. 3C-F) was effectively inhibited by Pyr3, an inhibitor of TRPC3-containing channels. Moreover, the mGluR1-induced Ca²⁺ rise in cultured PNs from WT mice was enhanced by the nNOS inhibitor 7N but decreased by the NO-donor SNAP and blocked by Pyr3 (Figs. 5C and D). We reason that the activity of STIM1-gated TRPC3-containing channels in PNs presenting in the cerebellar cell cultures was under constant restrictive control by NO from surrounding GNs and interneurons, which express nNOS [17]. Taken together, our results demonstrated that nNOS/NO signaling critically regulates the activity of TRPC3-containing channels hence EPSC_{Slow} in PNs. This idea was supported by the result that the conductance of TRPC3-containing channels in PNs from WT mice and nNOS^{-/-} was effectively reduced by the NO donor GSNO.

How does NO signaling inhibit the activity of TRPC3-containing channels thus constraining EPSC_{Slow} in PNs? Results from this study showed that PNs in both WT and nNOS^{-/-} mice displayed similar ratios of EPSC₂/EPSC₁

(Fig. 1C) and comparable amplitudes of EPSC_{Fast} (Fig. 1D). On the other hand, the ratio of EPSC_{Slow}/EPSC_{Fast} were drastically larger in nNOS^{-/-} mice than that in WT mice (Fig. 1H). Moreover, at the same concentration, mGluR1 agonist evoked significantly larger transmembrane conductance in cultured PNs from nNOS^{-/-} mice than that in PNs from WT mice (Figs. 3E and F). These results implied that the cerebellar nNOS/NO signaling effectively downregulates the mGluR1-initiated TRPC3-mediated EPSC_{Slow} in PNs by a mechanism independent of extracellular concentration of glutamate although it was reported to modulate presynaptic release [46] and astrocytic uptake [47] of glutamate. In addition, our result showed that nNOS deficiency did not increase the expression of total TRPC3 proteins in the cerebellum but mildly decreased the fluorescence intensity of TRPC3 in PNs (Fig. 2). Moreover, we previously demonstrated that the mGluR1 expression decreased in the cerebellum of nNOS^{-/-} mice [23]. Together, results from our studies indicate that amplification of the mGluR1-initiated TRPC3-containing-channel mediated EPSC_{Slow} in nNOS^{-/-} mice is not due to increased expressions of mGluR1 and TRPC3.

A way through which NO regulates cellular functions is to activate sGC, leading to production of cyclic GMP (cGMP) and activation of protein kinases G (PKG). Indeed, cerebellar PNs are endowed with the NO-sGC-cGMP-PKG signaling system [48] while individual PNs differentially regulate cGMP production [49]. However, the basal activity of PKG in PNs does not shape the EPSC_{Slow} [50] nor affect the TRPC3-mediated current in rats [51]. Therefore, it is unlikely that nNOS/NO downregulates the TRPC3-mediated EPSC_{Slow} in rodent cerebella through the sGC-cGMP-PKG pathway.

NO also regulates cellular functions by inducing S-nitrosylation of proteins [52], one of the post-translational protein modifications [53]. S-nitrosylation is a reversible, covalent addition of the NO moiety to cysteine thiols forming an S-nitrosoprotein (protein-SNO) plausibly through nitrosylases. Indeed, S-nitrosylation-dependent signaling in the cerebellum is essential for plasticity of PF-PN synapses [54]. In this regard, we have found that nNOS knockout increased the oligomers of STIM1 in PNs [23], and that nNOS/NO inhibits STIM1 oligomerization by S-nitrosylation of its Cys49 and Cys56 residues hence suppresses STIM1 mobilization and reduces the Orai1-channel current in mouse cardiomyocytes [43]. Therefore, we evaluated whether NO regulates TRPC3 channel activity by S-nitrosylation of STIM1 cysteine residues. Remarkably, our analyses showed that the TRPC3 conductance in HEK-293 cells co-expressing WT STIM1 and TRPC3 was significantly reduced by the NO-donor GSNO. In contrast, GSNO had no effect on the TRPC3 conductance in cells expressing STIM1 mutant (Cys49Ser and Cys56Ser) (Fig. 6). Together, these results implied that NO regulates

TRPC3-mediated cation current in PNs, at least partially, by S-nitrosylation of Cys49 and Cys56 at STIM1. We propose that under physiological conditions, basal NO induces S-nitrosylation STIM1 thus inhibits STIM1 oligomerization, consequently decreasing TRPC3 channel activity and limiting Ca^{2+} influx to PNs.

NO is a critical regulator of bidirectional plasticity at PF-PN synapses, inducing long-term depression (LTD) or long-term potentiation (LTP) depending on postsynaptic Ca^{2+} levels [55, 56], thus playing a pivotal role in cerebellum related motor controls [45]. Results from this study provide new knowledge of molecular mechanisms by which nNOS/NO regulates the PF-PN synaptic transmission. Specifically, our results for the first time demonstrated that basal nNOS/NO signaling in cerebellar cells restricts EPSC_{slow} hence limiting the mGluR1-initiated TRPC3-mediated entry of Ca^{2+} into PNs. These novel findings also help explain the abnormality of motor coordination in disease conditions of impaired cerebellar nNOS/NO signaling. For example, alcohol induces cerebellar neuronal injury [57] by inhibiting nNOS activity [58], whereas nNOS gene mutation worsens alcohol-induced cerebellar ataxia [59]. In addition, gain-function-mutation of TRPC3 results in ataxia [60] whereas reducing the mGluR1-initiated Ca^{2+} influx into PNs rescues ataxia in a mouse model of autosomal dominant cerebellar ataxia [61]. Therefore, whether appropriately increasing nNOS/NO signaling in the cerebellum improves motor coordination, speech, and cognitions of patients having cerebellar ataxia should be examined in the future.

Author contributions W-YL, WI, and QF proposed the study, and LG, VT, Y-YX, WI, and W-YL performed specific experiments. W-YL and WI wrote the manuscript.

Funding This study was supported by operating grants from the Canadian Institute of Health Research (MOP-133504 to W-YL).

Data Availability Not applicable.

Declarations

Ethical Approval All animal experimental procedures conform to the Canadian Council on Animal Care guidelines for the care and handling of animals and were approved by the Animal Care Committee at Western University under the AUP# 2010–033, AUP# 2014–031 and AUP#

Competing interests The authors declare no conflict of interest.

References

- Schmahmann JD, Guell X, Stoodley CJ, Halko MA. The Theory and Neuroscience of Cerebellar Cognition. *Annu Rev Neurosci*. 2019;42:337–64.
- Rancz EA, Ishikawa T, Duguid I, Chadderton P, Mahon S, et al. High-fidelity transmission of sensory information by single cerebellar mossy fibre boutons. *Nature*. 2007;450:1245–8.
- Arenz A, Silver RA, Schaefer AT, Margrie TW. The contribution of single synapses to sensory representation in vivo. *Science*. 2008;321:977–80.
- Batchelor AM, Garthwaite J. Frequency detection and temporally dispersed synaptic signal association through a metabotropic glutamate receptor pathway. *Nature*. 1997;385:74–7.
- Canepari M, Papageorgiou G, Corrie JE, Watkins C, Ogden D. The conductance underlying the parallel fibre slow EPSP in rat cerebellar Purkinje neurones studied with photolytic release of L-glutamate. *J Physiol*. 2001;533:765–72.
- Hartmann J, Dragicevic E, Adelsberger H, Henning HA, Sumser M, et al. TRPC3 channels are required for synaptic transmission and motor coordination. *Neuron*. 2008;59:392–8.
- Canepari M, Auger C, Ogden D. Ca^{2+} ion permeability and single-channel properties of the metabotropic slow EPSC of rat Purkinje neurons. *J Neurosci*. 2004;24:3563–73.
- Becker EB, Oliver PL, Glitsch MD, Banks GT, Achilli F, et al. A point mutation in TRPC3 causes abnormal Purkinje cell development and cerebellar ataxia in moonwalker mice. *Proc Natl Acad Sci U S A*. 2009;106:6706–11.
- Skibinska-Kijek A, Wisniewska MB, Gruszczynska-Biegala J, Methner A, Kuznicki J. Immunolocalization of STIM1 in the mouse brain. *Acta Neurobiol Exp (Wars)*. 2009;69:413–28.
- Zeng W, Yuan JP, Kim MS, Choi YJ, Huang GN, et al. STIM1 gates TRPC channels, but not Orai1, by electrostatic interaction. *Mol Cell*. 2008;32:439–48.
- Lee KP, Choi S, Hong JH, Ahuja M, Graham S, et al. Molecular determinants mediating gating of Transient Receptor Potential Canonical (TRPC) channels by stromal interaction molecule 1 (STIM1). *J Biol Chem*. 2014;289:6372–82.
- Hartmann J, Karl RM, Alexander RP, Adelsberger H, Brill MS, et al. STIM1 controls neuronal Ca^{2+} signaling, mGluR1-dependent synaptic transmission, and cerebellar motor behavior. *Neuron*. 2014;82:635–44.
- Jin Y, Kim SJ, Kim J, Worley PF, Linden DJ. Long-term depression of mGluR1 signaling. *Neuron*. 2007;55:277–87.
- Ishibashi K, Miura Y, Ishikawa K, Zhang MR, Toyohara J, et al. Relationship between type 1 metabotropic glutamate receptors and cerebellar ataxia. *J Neurol*. 2016;263:2179–87.
- Shuvaev AN, Hosoi N, Sato Y, Yanagihara D, Hirai H. Progressive impairment of cerebellar mGluR signalling and its therapeutic potential for cerebellar ataxia in spinocerebellar ataxia type 1 model mice. *J Physiol*. 2017;595:141–64.
- Egorova PA, Marinina KS, Bezprozvanny IB. Chronic suppression of STIM1-mediated calcium signaling in Purkinje cells rescues the cerebellar pathology in spinocerebellar ataxia type 2. *Biochim Biophys Acta Mol Cell Res*. 2023;1870: 119466.
- Abbott LC, Nahm SS. Neuronal nitric oxide synthase expression in cerebellar mutant mice. *Cerebellum*. 2004;3:141–51.
- Broillet MC. S-nitrosylation of proteins. *Cell Mol Life Sci*. 1999;55:1036–42.
- Linden DJ, Dawson TM, Dawson VL. An evaluation of the nitric oxide/cGMP/cGMP-dependent protein kinase cascade in the induction of cerebellar long-term depression in culture. *J Neurosci*. 1995;15:5098–105.
- Lev-Ram V, Nebyelul Z, Ellisman MH, Huang PL, Tsien RY. Absence of cerebellar long-term depression in mice lacking neuronal nitric oxide synthase. *Learn Mem*. 1997;4:169–77.
- Kriegsfeld LJ, Eliasson MJ, Demas GE, Blackshaw S, Dawson TM, et al. Nocturnal motor coordination deficits in neuronal nitric oxide synthase knock-out mice. *Neuroscience*. 1999;89:311–5.
- Katoh A, Kitazawa H, Itohara S, Nagao S. Inhibition of nitric oxide synthesis and gene knockout of neuronal nitric oxide

- synthase impaired adaptation of mouse optokinetic response eye movements. *Learn Mem.* 2000;7:220–6.
23. Tellios V, Maksoud MJE, Xiang YY, Lu WY. Nitric Oxide Critically Regulates Purkinje Neuron Dendritic Development Through a Metabotropic Glutamate Receptor Type 1-Mediated Mechanism. *Cerebellum.* 2020;19:510–26.
 24. Llano I, Marty A, Armstrong CM, Konnerth A. Synaptic- and agonist-induced excitatory currents of Purkinje cells in rat cerebellar slices. *J Physiol.* 1991;434:183–213.
 25. Dzubay JA, Otis TS. Climbing fiber activation of metabotropic glutamate receptors on cerebellar purkinje neurons. *Neuron.* 2002;36:1159–67.
 26. Konnerth A, Llano I, Armstrong CM. Synaptic currents in cerebellar Purkinje cells. *Proc Natl Acad Sci U S A.* 1990;87:2662–5.
 27. Yu F, Zhong P, Liu X, Sun D, Gao HQ, et al. Metabotropic glutamate receptor I (mGluR1) antagonism impairs cocaine-induced conditioned place preference via inhibition of protein synthesis. *Neuropsychopharmacology.* 2013;38:1308–21.
 28. Abdoul-Azize S, Buquet C, Vannier JP, Dubus I. Pyr3, a TRPC3 channel blocker, potentiates dexamethasone sensitivity and apoptosis in acute lymphoblastic leukemia cells by disturbing Ca(2+) signaling, mitochondrial membrane potential changes and reactive oxygen species production. *Eur J Pharmacol.* 2016;784:90–8.
 29. Maksoud MJE, Tellios V, An D, Xiang YY, Lu WY. Nitric oxide upregulates microglia phagocytosis and increases transient receptor potential vanilloid type 2 channel expression on the plasma membrane. *Glia.* 2019;67:2294–311.
 30. Januzi L, Poirier JW, Maksoud MJE, Xiang YY, Veldhuizen RAW, et al. Autocrine GABA signaling distinctively regulates phenotypic activation of mouse pulmonary macrophages. *Cell Immunol.* 2018;332:7–23.
 31. Dong H, Kumar M, Zhang Y, Gyulkhandanyan A, Xiang YY, et al. Gamma-aminobutyric acid up- and downregulates insulin secretion from beta cells in concert with changes in glucose concentration. *Diabetologia.* 2006;49:697–705.
 32. Feng AL, Xiang YY, Gui L, Kaltsidis G, Feng Q, et al. Paracrine GABA and insulin regulate pancreatic alpha cell proliferation in a mouse model of type 1 diabetes. *Diabetologia.* 2017;60:1033–42.
 33. Baptista CA, Hatten ME, Blazeski R, Mason CA. Cell-cell interactions influence survival and differentiation of purified Purkinje cells in vitro. *Neuron.* 1994;12:243–60.
 34. Morrison ME, Mason CA. Granule neuron regulation of Purkinje cell development: striking a balance between neurotrophin and glutamate signaling. *J Neurosci.* 1998;18:3563–73.
 35. Chen WK, Liu IY, Chang YT, Chen YC, Chen CC, et al. Ca(v)3.2 T-type Ca2+ channel-dependent activation of ERK in paraventricular thalamus modulates acid-induced chronic muscle pain. *J Neurosci.* 2010;30:10360–8.
 36. Schindelin J, Arganda-Carreras I, Frise E, Kaynig V, Longair M, et al. Fiji: an open-source platform for biological-image analysis. *Nat Methods.* 2012;9:676–82.
 37. Stathopoulos PB, Zheng L, Li GY, Plevin MJ, Ikura M. Structural and mechanistic insights into STIM1-mediated initiation of store-operated calcium entry. *Cell.* 2008;135:110–22.
 38. Lavreysen H, Wouters R, Bischoff F, Nobrega Pereira S, Langlois X, et al. JNJ16259685, a highly potent, selective and systemically active mGlu1 receptor antagonist. *Neuropharmacology.* 2004;47:961–72.
 39. Kiyonaka S, Kato K, Nishida M, Mio K, Numaga T, et al. Selective and direct inhibition of TRPC3 channels underlies biological activities of a pyrazole compound. *Proc Natl Acad Sci U S A.* 2009;106:5400–5.
 40. Wu B, Blot FG, Wong AB, Osorio C, Adolfs Y, et al. (2019) TRPC3 is a major contributor to functional heterogeneity of cerebellar Purkinje cells. *Elife* 8. <https://doi.org/10.7554/eLife.45590>
 41. Harbers M, Nakao H, Watanabe T, Matsuyama K, Tohyama S, et al. (2022) mGluR5 Is Substitutable for mGluR1 in Cerebellar Purkinje Cells for Motor Coordination, Developmental Synapse Elimination, and Motor Learning. *Cells* 11. <https://doi.org/10.3390/cells11132004>
 42. Sukumaran P, Sun Y, Vyas M, Singh BB. TRPC1-mediated Ca(2+) (+) entry is essential for the regulation of hypoxia and nutrient depletion-dependent autophagy. *Cell Death Dis.* 2015;6: e1674.
 43. Gui L, Zhu J, Lu X, Sims SM, Lu WY, et al. S-Nitrosylation of STIM1 by Neuronal Nitric Oxide Synthase Inhibits Store-Operated Ca(2+) Entry. *J Mol Biol.* 2018;430:1773–85.
 44. Zhang J, Yuan H, Yao X, Chen S. Endogenous ion channels expressed in human embryonic kidney (HEK-293) cells. *Pflugers Arch.* 2022;474:665–80.
 45. Contestabile A. Role of nitric oxide in cerebellar development and function: focus on granule neurons. *Cerebellum.* 2012;11:50–61.
 46. Marcoli M, Cervetto C, Paluzzi P, Guarnieri S, Raiteri M, et al. Nitric oxide-evoked glutamate release and cGMP production in cerebellar slices: control by presynaptic 5-HT1D receptors. *Neurochem Int.* 2006;49:12–9.
 47. Tellios V, Maksoud MJE, Lu WY. The expression and function of glutamate aspartate transporters in Bergmann glia are decreased in neuronal nitric oxide synthase-knockout mice during postnatal development. *Glia.* 2022;70:858–74.
 48. Endo S, Suzuki M, Sumi M, Nairn AC, Morita R, et al. Molecular identification of human G-substrate, a possible downstream component of the cGMP-dependent protein kinase cascade in cerebellar Purkinje cells. *Proc Natl Acad Sci U S A.* 1999;96:2467–72.
 49. Shimizu-Albergine M, Rybalkin SD, Rybalkina IG, Feil R, Wolfgruber W, et al. Individual cerebellar Purkinje cells express different cGMP phosphodiesterases (PDEs): in vivo phosphorylation of cGMP-specific PDE (PDE5) as an indicator of cGMP-dependent protein kinase (PKG) activation. *J Neurosci.* 2003;23:6452–9.
 50. Canepari M, Ogden D. Evidence for protein tyrosine phosphatase, tyrosine kinase, and G-protein regulation of the parallel fiber metabotropic slow EPSC of rat cerebellar Purkinje neurons. *J Neurosci.* 2003;23:4066–71.
 51. Nelson C, Glitsch MD. Lack of kinase regulation of canonical transient receptor potential 3 (TRPC3) channel-dependent currents in cerebellar Purkinje cells. *J Biol Chem.* 2012;287:6326–35.
 52. Hess DT, Stamler JS. Regulation by S-nitrosylation of protein post-translational modification. *J Biol Chem.* 2012;287:4411–8.
 53. Anand P, Stamler JS. Enzymatic mechanisms regulating protein S-nitrosylation: implications in health and disease. *J Mol Med (Berl).* 2012;90:233–44.
 54. Kakizawa S, Shibasaki M, Mori N. Protein oxidation inhibits NO-mediated signaling pathway for synaptic plasticity. *Neurobiol Aging.* 2012;33:535–45.
 55. Wang DJ, Su LD, Wang YN, Yang D, Sun CL, et al. Long-term potentiation at cerebellar parallel fiber-Purkinje cell synapses requires presynaptic and postsynaptic signaling cascades. *J Neurosci.* 2014;34:2355–64.
 56. Lev-Ram V, Jiang T, Wood J, Lawrence DS, Tsien RY. Synergies and coincidence requirements between NO, cGMP, and Ca2+ in the induction of cerebellar long-term depression. *Neuron.* 1997;18:1025–38.
 57. Bookstein FL, Streissguth AP, Connor PD, Sampson PD. Damage to the human cerebellum from prenatal alcohol exposure: the anatomy of a simple biometrical explanation. *Anat Rec B New Anat.* 2006;289:195–209.
 58. Fataccioli V, Gentil M, Nordmann R, Rouach H. Inactivation of cerebellar nitric oxide synthase by ethanol in vitro. *Alcohol Alcohol.* 1997;32:683–91.

59. Bonthius DJ Jr, Winters Z, Karacay B, Bousquet SL, Bonthius DJ. Importance of genetics in fetal alcohol effects: null mutation of the nNOS gene worsens alcohol-induced cerebellar neuronal losses and behavioral deficits. *Neurotoxicology*. 2015;46:60–72.
60. Fogel BL, Hanson SM, Becker EB. Do mutations in the murine ataxia gene TRPC3 cause cerebellar ataxia in humans? *Mov Disord*. 2015;30:284–6.
61. Maltecca F, Baseggio E, Consolato F, Mazza D, Podini P, et al. Purkinje neuron Ca²⁺ influx reduction rescues ataxia in SCA28 model. *J Clin Invest*. 2015;125:263–74.

Publisher's Note Springer Nature remains neutral with regard to jurisdictional claims in published maps and institutional affiliations.

Springer Nature or its licensor (e.g. a society or other partner) holds exclusive rights to this article under a publishing agreement with the author(s) or other rightsholder(s); author self-archiving of the accepted manuscript version of this article is solely governed by the terms of such publishing agreement and applicable law.